PROCEEDINGS

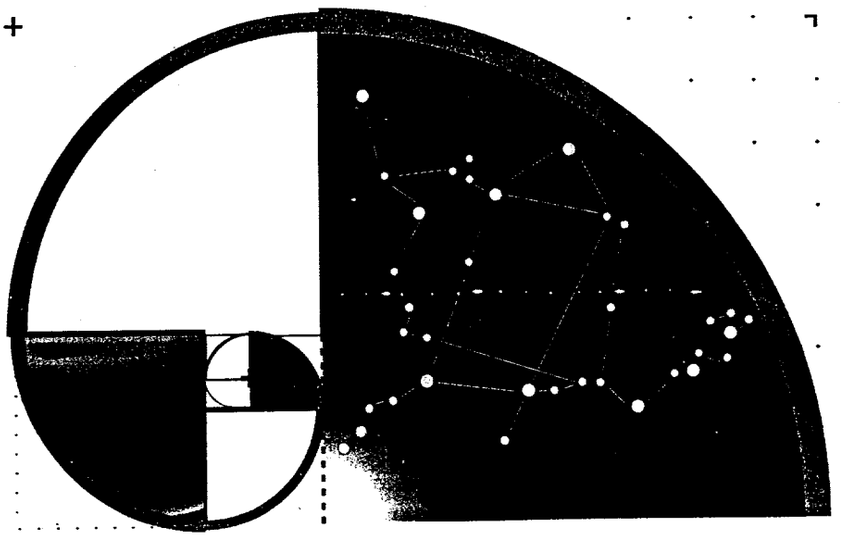

N A S A

U C
UNIVERSITY OF
CINCINNATI

SPACE
ENGINEERING
CENTER
FOR SYSTEM HEALTH MANAGEMENT TECHNOLOGY

FOURTH ANNUAL SPACE SYSTEM HEALTH MANAGEMENT TECHNOLOGY CONFERENCE

OMNI NETHERLAND PLAZA HOTEL CINCINNATI, OHIO

NOVEMBER 17TH - 18TH 1992.

SSME Mainstage Sensor Signal Approximation Using Feedforward Neural Networks[1,2]

Claudia M. Meyer and William A. Maul
Sverdrup Technology, Inc.
Lewis Research Center Group
Cleveland, OH 44212
(216)-977-7511

Atam P. Dhawan
University of Cincinnati
Department of Electrical and Computer Engineering
Cincinnati, OH 45221

Abstract

Feedforward neural networks with two hidden layers were used to approximate two redlined parameters during mainstage operation of the space shuttle main engine. The parameters were the high pressure oxidizer turbine and high pressure fuel turbine discharge temperatures. Accurate models of critical parameters are needed for real-time and post-test sensor validation. A standard backpropagation algorithm was used to train the networks on data from two nominal firings. The trained networks were validated using data from five additional nominal firings. The ability of the trained networks to accurately predict the two redlined parameters was shown. The performance of the trained networks in the event of an input sensor failure was characterized; good prediction accuracy was maintained when the failed sensor measurement was replaced with a synthesized value from another network.

Nomenclature

a	activation function of hidden and output layer nodes
CADS	command and data simulator
e(t)	error or residual
f	nonlinear function describing relationship between system variables
FPB	fuel preburner
FPOV	fuel preburner oxidizer valve
HPFT	high pressure fuel turbine
HPFP	high pressure fuel pump
HPOT	high pressure oxidizer turbine
HPOTP	high pressure oxidizer turbopump
lox	liquid oxygen
MCC	main combustion chamber
n_i	window size of function input variable $u_i(t)$
net_i	the net input to node i
o_i	the output of node i

---

[2]This work was sponsored, in part, by OAST Space Transportation through NASA Lewis Research Center contract NAS3-25266.

OPB	oxidizer preburner
OPOV	oxidizer preburner oxidizer valve
PBP	preburner boost pump
PID	parameter identification
r	number of model input variables
rms	root mean squared
RPL	rated power level
SSME	space shuttle main engine
$u_i(t)$	a function input variable
w_{ij}	weight connecting nodes i and j in adjacent layers
y(t)	the function output

Introduction

Multilayer feedforward neural networks were used to approximate two critical parameters during mainstage operation of the Space Shuttle Main Engine (SSME). The two parameters selected were the High Pressure Fuel Turbine (HPFT) and the High Pressure Oxidizer Turbine (HPOT) discharge temperatures; both are redlined parameters. The trained neural networks, or models, were developed for eventual inclusion in the sensor validation module of a real-time advanced safety system or an automated post-test diagnostic system. The errors, or differences between the actual sensor values and the neural network model predicted values provide information on the health of the sensor suite under consideration.

Sensors fail at a much higher rate than any other component class on the SSME.[1] Despite sensor reasonableness checks conducted by the SSME controller on redlined and controlled parameters, failures of redlined sensors have been responsible for premature engine cutoffs during ground test firings and flight. The failure of both HPFT discharge temperature sensors on one engine during space shuttle mission 51F caused that SSME to erroneously cutoff; the mission was completed after an abort-to-orbit.[1] As advanced safety algorithms are developed and tested,[2,3] validation of a large number of performance sensors has become necessary. Sensor validation is also a vital component of an automated post-test diagnostic system since failed sensors must be identified before engine health assessments can be made.[4]

Several approaches to SSME sensor validation have been identified.[5,6] Most involve analytical redundancy, the use of redundant information from dissimilar sensors to approximate the sensor in question. Some function approximation techniques are based on first principle relationships while others are empirically derived. Neural networks are especially attractive for approximating complex nonlinear systems such as the SSME since they can uniformly approximate any continuous function.[7,8] In addition, neural networks are well-suited for real-time monitoring because of their highly parallel architecture. Autoassociative networks have been used for sensor failure detection and recovery of simulated SSME data.[9] Multiple input, single output feed-forward networks have been used to model critical parameters during the SSME startup transient; actual test data was used for training and validation.[10]

In this investigation, Command and Data Simulator (CADS) and facility data were used to approximate the relationships among several SSME sensor measurements during mainstage operation of the engine; all power levels and power-level transitions following startup and prior to shutdown were included. All data used for network training and validation were taken from test firings on the B1 test stand at Stennis Space Center: B1060, B1061, B1062, B1063, B1066, B1067, and B1069. Multiple input, single output networks were trained using the backpropagation algorithm. Several issues regarding the training and use of the networks were addressed. These included the selection of measurements for use as network inputs, the selection of training data, the behavior of the trained networks in the event of an input sensor failure, and the use of synthesized inputs. Several error statistics were used to characterize the performance of the trained networks: standard deviation of the error, mean error, maximum error and maximum percent error.

Analysis

Theory

The mathematical relationship between observed system variables, or sensor outputs, can be very complex and the exact form is usually unknown. In practice, the modeling of real-world systems based on observed system variables is achieved by choosing a model set of known functions that is dense in the space of continuous functions.[11] Polynomial functions are an example of such a model set. Feedforward networks with nonlinear processing elements have been considered as an alternative model set and have been successfully used to model nonlinear dynamic systems.[9-12] Because neural networks can uniformly approximate any continuous function, the neural network approach has some advantages over more conventional methods. Polynomial methods, for example, have difficulties in the presence of nonpolynomial nonlinearities while neural networks can accurately model both polynomial and nonpolynomial nonlinearities.[12]

Consider the nonlinear function, *f*, that describes the relationship between several system variables:

$$y(t)=f(u_1(t-1),\ldots,u_1(t-n_1),u_2(t-1),\ldots,u_2(t-n_2),\ldots,u_i(t-1),\ldots,u_i(t-n_i),\ldots,u_r(t-1),\ldots,u_r(t-n_r))+e(t) \quad (1)$$

where y(t) is the parameter to be approximated, $u_i(t)$ is a function input variable, n_i is the window size for input variable $u_i(t)$, and e(t) is the error or residual.[11] The window size, n_i, refers to the number of past time slices of u_i which are used as function inputs. The total number of input variables is r. Neural networks are trained to approximate the function *f* based on observed system variables, $u_i(t)$ and y(t).

A feedforward neural network consists of layers of processing elements called nodes. Each node of a given layer receives input from all of the nodes in the previous layer and sends its output to each node in the following layer. The connections are unidirectional and have weights associated with them. There are no connections between nodes within a layer and no connections bridging layers. The relationship between the input and the output of a node in the hidden or output layers is determined by the activation function, *a*. The commonly used sigmoid activation function was employed in this study:[13]

$$a(net_i)=o_i=\frac{1}{1+e^{-net_i}}-\frac{1}{2} \quad (2)$$

where net_i is the net input to node i

$$net_i=\theta_i+\Sigma w_{ij}o_j \quad (3)$$

θ_i is the bias term for node i, o_j is the output of node j in the previous layer, and w_{ij} is the weight between the two nodes i and j. A bias is similar in principle to a threshold and is treated as a weight connected to a node that is always on.

The values of the weights and biases are adjusted during the learning process. The networks were trained using the backpropagation algorithm, a supervised learning procedure based on the Generalized Delta Rule.[16] Backpropagation computes the weights and bias terms to minimize the mean squared error between the desired values and the values predicted by the network. In this investigation, the weights and biases were updated after every training pattern. A neural network training pattern consists of a desired output and all of the inputs associated with that output. The learning rate and momentum determined the amount by which the weights were updated and were set to achieve rapid learning without significant oscillations in the error.[16]

It has been mathematically proven that a three-layer feedforward network (an input layer, a hidden layer, and an output layer) with sigmoidal activation nodes can uniformly approximate any continuous function.[7,8] Unfortunately, no guidelines exist as to the number of hidden nodes required to provide a satisfactory solution. For many problems, an approximation with three layers would require an impractically large number of hidden

nodes.[14] It is generally thought that additional hidden layers can realize a given mapping with less cost (smaller networks and subsequently shorter training times) than one hidden layer.[7,14,15] For this reason, two hidden layers were used in this investigation.

Four parameters were used to assess the performance of the trained networks. The mean output error represents the average offset of the error from zero during a given training or validation set. The standard deviation represents the variation of the error about this mean. The maximum error represents the maximum difference (absolute value) between actual and predicted values and the maximum percent error is the maximum percent difference (absolute value) between actual and predicted values during a given training or validation set.

Application to SSME Data

The neural network models developed in this investigation are to analyze the SSME data prior to passing the data to a safety system or an automated post-test diagnostic system. Figure 1 shows the flow of data from the engine and highlights the major features of the sensor validation module. The neural network models will provide predicted values which can be compared to actual values in order to make sensor health assessments. A set of validated measurements is passed on for use by a real-time safety system or post-test diagnostic system. In the event of a sensor failure, predicted values will be used for that parameter wherever it appears as a model input. This section addresses the issues associated with the development of the neural network models: selection of inputs, construction of the training set, and selection of a network architecture.

The selection of neural network inputs was largely based on knowledge of the engine cycle and the availability of instrumentation. In addition to sensor measurements, two combinations of sensor measurements were used as inputs to the turbine discharge temperature models in order to improve model prediction accuracy. The first consisted of the difference between the controller reference chamber pressure and the actual chamber pressure. Deviations in this combined parameter from zero indicate the onset of a power-level transition. The second combined parameter was a 1-sec average of the measurement being modeled. The 1-sec average was computed at the onset of mainstage and was used as an additional model input for the remainder of the test firing. This combined parameter was used to anchor the network to the particular test firing in question so that the model would be desensitized to changes in hardware or test conditions which are not directly measured. Although such changes do not affect the relationships between parameters, they do affect parameter magnitudes, causing some parameters to experience large test-to-test variations.

Network size was another factor that contributed to the selection of the input set. A small number of inputs, and hence a smaller network, was desired to reduce network training times and to facilitate the sensor fault isolation process. A systematic methodology for the selection of an optimal or near-optimal set of inputs is currently being investigated.[17] In this investigation, a small set of parameters physically related to the parameter being modeled was selected. The final input sets for each of the turbine discharge temperatures are given in Table 1. Parameter Identification (PID) numbers are also included in this table.

The window size, n_i, for each input variable was also influenced by network size considerations. In modeling the startup transient, window sizes were used to improve model prediction accuracy.[10] Due to the largely steady-state nature of mainstage operation and the slow sampling rate of CADS and facility data, a window size consisting of one time slice was feasible in this study. Thus, n_i in Eq. (1) was equal to one for all input parameters; measurements at time t-1 were used to predict measurements at time t. Since the sampling rate of the CADS data was 25 Hz, t-1 referred to the sample 40 msec earlier than the current time slice. The use of the t-1 value also facilitated the substitution of a synthesized signal in the event of a sensor failure.

The training sets for the neural network models were taken from two nominal test firings on the B1 test stand. B1060 and B1063 were selected so that all power levels would be included in training: 65% Rated Power Level (RPL), 100% RPL, 104% RPL and 109% RPL. Furthermore, both of these tests included liquid oxygen (lox) side venting, a phenomenon that complicates the approximation of the turbine discharge

temperatures by introducing non-stationary behavior during constant power-level intervals. Since both tests were long in duration (530 and 513 sec, respectively) training patterns were created only for every fifth value of the output parameter. This made the size of the training sets more manageable. Prior to training, all inputs and outputs were normalized to fall within the range [-0.5, 0.5] as dictated by the activation function given by Eq. (2). The normalization was achieved by selecting minimum and maximum values for the input and output parameters based on the data contained in approximately twenty test firings. Finally, the training patterns were randomized prior to training; this greatly enhanced training efficiency since the weights were updated after every training pattern.

For reasons stated in the previous section, feedforward neural networks with two hidden layers were used to approximate the turbine discharge temperatures. The HPOT discharge temperature had a total of seven input nodes and the HPFT discharge temperature had eight. Both networks had ten nodes in the first hidden layer, five nodes in the second hidden layer, and one output node for the parameter being modeled. Although the node selections were somewhat arbitrary, it was found that increasing the number of nodes in the hidden layers greatly increased the training times without showing improved performance on the training or validation firings. The network architecture used to model the HPOT discharge temperature is shown in Figure 2; the input nodes have been labeled with their corresponding PID numbers. All connections between nodes are shown. Both networks were trained until no appreciable decrease in the rms error was observed, approximately 10000 training cycles.

Results and Discussion

Data from two nominal firings, B1060 and B1063, were used to train neural networks to predict the HPOT and HPFT discharge temperatures during mainstage operation of the SSME. After training, the networks were tested on five additional nominal firings on the same test stand: B1061, B1062, B1066, B1067 and B1069. In addition, sensor failures were injected at specified times during the validation firings in order to demonstrate the impact of a failed input on the neural network output. When the HPOT discharge temperature was failed, its neural network model predicted value was used in the input to the HPFT discharge temperature model. The behavior of the networks with faulty and synthesized inputs was characterized to establish the usefulness of the neural network models in the event of an input sensor failure. Only " hard sensor failures" were considered; the sensor in question malfunctioned and remained unresponsive to true engine conditions for the remainder of the test.

The results presented in this section will be illustrated using one of the validation firings, B1066. The power-level profile for this test firing is representative of the training and validation firing power-level profiles and is shown in Figure 3. Although the engine fires at 104% RPL for a majority of this test firing, shorter intervals at 100% RPL, 104% RPL and 65% RPL can also be seen. Lox tank venting and repressurization commenced at 80 sec during this test firing and ended at 500 sec. All training and validation test firings experienced lox tank venting and repressurization.

Figure 4 gives an example of the performance of the trained HPOT discharge temperature network on validation test firing B1066. Actual and predicted values are given in Fig. 4(a), and Fig. 4(b) shows the error, or difference between the two curves. As can be seen, the predicted value and the actual value are very close during the extended 104% RPL interval; the effects of lox venting are evident during this interval and are accurately reproduced by the model. Venting is responsible for the non-stationary behavior seen in Fig. 4(a) during 104% RPL. In general, the largest errors were found in the beginning of the validation firings when considerable variability is observed in many engine parameters. The large flow, pressure and temperature gradients associated with startup and the frequent power-level transitions early in the test firing prevent many parameters from attaining steady-state behavior during the early portions of mainstage operation.

Figure 4(b) also shows that the largest error of extended duration occurred during the throttle down to 65% RPL. It should be noted that, like B1066, the training test firings contained little data at 65% RPL. An

attempt to take more data from these short intervals (every point or every other point as opposed to every fifth point) did not improve the error statistics of the trained networks at 65% RPL or in general. These observations indicate that it may be appropriate to make error thresholds a function of power level. Furthermore, the large spikes in the error all coincide with power-level transitions. In addition to taking these power-level changes into account when applying thresholds, a multi-sampling-interval decision strategy should be used to avoid false alarms. For example, exceedance of the error threshold on two of three consecutive sampling intervals may be required to declare a sensor failure.

A summary of the performance of the trained network on all validation firings is given in Table 2. Several points regarding the residual statistics are noteworthy. The largest maximum percent error is 6.2%. As described above, a multi-cycle decision strategy would reduce the importance of any single error and would focus on large errors in consecutive sampling intervals. The percent error for B1066 is shown in Fig. 5. As can be seen, the percent error is typically less than three percent in absolute value. The mean residual and standard deviation of the residual are higher for test firings B1067 and B1069. These tests were both 750 sec in duration; very long duration tests typically exhibit different behavior as the hardware reaches thermal equilibrium. The error plots are consistent with this observation since the average difference between actual and predicted values was found to increase as a function of time for these two test firings. Training on long duration tests may alleviate this problem.

Figure 6 gives an example of the performance of the HPFT discharge temperature network on the same validation test firing, B1066. The actual and predicted values are shown in Fig. 6(a), and the errors are given in Fig. 6(b). The HPFT discharge temperature does not experience nearly as much variability as the HPOT discharge temperature early in mainstage and is not as strongly affected by venting. As with the HPOT discharge temperature prediction, the largest offset of a significant duration occurs during the 65% power level. A summary of the performance of the HPFT discharge temperature network on the validation firings is given in Table 3. As for the HPOT discharge temperature, larger errors are observed for the long-duration test firings, B1067 and B1069. The maximum percent errors for the HPOT discharge temperature network are between two and four times larger than for the HPFT discharge temperature network. This is partially due to the smaller variability of the HPFT discharge temperature cited previously. Furthermore, the fuel side of the SSME is more heavily instrumented; thus, there is better redundant information available to model the fuel turbine discharge temperature.

Once the performance of the trained networks had been established with nominal data, inputs to the HPFT discharge temperature model were failed. This model was selected since it uses the HPOT discharge temperature as an input. Therefore, when the HPOT discharge temperature sensor fails, a synthesized value is available for substitution from the trained neural network model for this parameter. Two examples of the impact of an input failure on the HPFT discharge temperature prediction are given in Fig. 7. In both cases, the "hard sensor failure" was injected at t=175 sec. Figure 7(a) shows the actual and predicted values for the HPFT discharge temperature when the HPOT discharge temperature was failed at t=175 sec. The HPOT discharge temperature was assumed to have a constant value of 2760 deg R, the upper limit for this temperature sensor.[18] The impact of the input sensor failure is immediately evident. The result of failing the Main Combustion Chamber (MCC) coolant discharge pressure at t=175 sec is shown in Fig. 7(b); the MCC discharge pressure was assumed to have a failed value of 14.7 psia (ambient, meaning that the sensor had not been hooked up). It was found that injecting a hard failure for any input had an immediate impact on the predicted value.

In the case of a failed HPOT discharge temperature sensor, the HPOT discharge temperature model was available to provide a synthesized input for the HPFT discharge temperature model. Figure 8 shows the effect of substituting the predicted value for the actual value at t=175 sec. Figures 8(a) and 8(b) can be compared to Fig. 6(a) and 6(b) which used the actual data for the HPOT discharge temperature. The residual plots are very similar. The mean error when using the actual data for the HPOT discharge was 5.2 deg R, while the mean error when using the synthesized value was 5.8 deg R. The standard deviation increased slightly from 5.7 deg R to 5.8 deg R when the synthesized value was used for the HPOT discharge temperature. The maximum error

and maximum percent error (absolute value in both cases) remained unchanged since they occurred prior to the substitution of the synthesized parameter. The continued good performance of the neural network models with a synthesized input was essential. If a sensor which appeared in the input of a large number of models failed, substituting a synthesized value for the failed sensor's measurement would ensure the continued usefulness of these models.

Concluding Remarks

Feedforward neural networks with two hidden layers can be used to provide accurate predictions for critical SSME parameters during mainstage operation of the engine. Such models provide analytical redundancy for use in detecting and isolating failed instrumentation. Automated sensor validation is crucial for a safety system in order to prevent erroneous cutoffs due to sensor failures and for a post-test diagnostic system which must make engine and sensor health assessments.

The models in this investigation were developed and tested using seven test firings on the B1 test stand. Model input parameters were selected based on knowledge of the engine cycle and instrumentation availability. The largest percent error for the HPOT discharge temperature was 6.2 percent while the largest percent error for the HPFT discharge temperature was 2.5 percent. Better prediction accuracy is possible for the HPFT discharge temperature because more instrumentation is available on the fuel side of the engine and because this parameter experiences less variability than the HPOT discharge temperature.

Larger errors were observed early in the test firings and during power-level transitions. The nature of the errors suggests the use of power-level dependent thresholds and multi-sampling-interval decision strategies in order to avoid false alarms. Long test firings were observed to exhibit slowly increasing errors as a function of time. This problem may be alleviated through the use of different training test firings. The selection of training data will be crucial as neural network models are developed for engines on all test stands.

A hard failure of a model input was found to immediately impact the accuracy of the predicted value. However, when a synthesized value was available for substitution, the prediction accuracy of the model was comparable to when actual nominal data were used. Thus, the models would continue to provide predicted values for sensor fault detection and isolation after the identification of a failed sensor.

In addition to providing information to make sensor health assessments, analytical redundancy techniques provide a predicted value which can be used for continued real-time or post-test monitoring in the event of a sensor failure. The availability of synthesized signals may be critical for space-based engine safety systems since the entire engine is anticipated to be the orbital replaceable unit; therefore, individual sensors cannot be replaced.

References

1. Wong, K. *Space Shuttle Sensor Assessment,* Vitro Corporation, Internal NASA HQ Report, April 1990.

2. Ruiz, C.A.; Hawman, M.W.; and Galinaitis, W.S. Algorithms for Real-Time Fault Detection of the Space Shuttle Main Engine. *AIAA Paper 92-3167,* July 1992.

3. Norman, A.; Maram, J.; Coleman, P.; Valentine, M.; and Steffens, A. Development of a Real-Time Model Based Safety Monitoring System Algorithm for the SSME. *AIAA Paper-92-3165,* July 1992.

4. Zakrajsek, J.F. The Development of a Post-Test Diagnostic System for Rocket Engines. *AIAA Paper 91-2528,* June 1991.

5. Makel, D.K.; Flaspohler, W.H.; and Bickmore, T.W. Sensor Data Validation and Reconstruction, Phase 1: System Architecture Study. *NASA CR-187122,* 1991.

6. Bickmore, T. Probabilistic Approach to Sensor Data Validation. *AIAA 92-3163*, July 1992.

7. Funahashi, K. On the Approximate Realization of Continuous Mappings by Neural Networks. *Neural Networks*, vol. 2, 1989, pp. 183-192.

8. Hornik, K.; Stinchcombe, M.; and White, H. Multilayer Feedforward Networks are Universal Approximators. *Neural Networks*, vol. 2, 1989, pp. 359-366.

9. Lin, C.S.; Wu, I.C.; and Guo, T.H. Neural Networks for Sensor Failure Detection and Data Recovery. *Proceedings of International Conference on Artificial Neural Networks in Engineering*, St. Louis, November 10-12, 1991.

10. Meyer, C.M. and Maul, W.A. The Application of Neural Networks to the SSME Startup Transient. *AIAA Paper 91-2530*, June 1991.

11. Chen, S., Billings, S.A., and Grant, P.M. Non-linear Systems Identification Using Neural Networks. *University of Edinburgh Research Report 370*, August 1989.

12. Lapedes, A. and Farber, R. Nonlinear Signal Processing Using Neural Networks: Prediction and System Modelling. *Los Alamos National Laboratory Technical Report LA-UR-87-2662*, July 1987.

13. *ANSim User's Manual, Version 2.30.* Science Applications International Corporation, April 1989.

14. Hecht-Neilsen. *Neurocomputing*. Addison-Wesley Publishing Company, Inc., 1990.

15. Lapedes, A. and Farber, R. How Neural Nets Work. In *Neural Information Processing Systems*, D.Z. Anderson, ed. New York: American Institute of Physics, 1988.

16. Rumelhart, D.E. and McClelland, J.L. *Parallel Distributed Processing: Explorations in the Microstructure of Cognition, I.* Cambridge, MA: MIT Press, 1987.

17. Peck, C.; Dhawan, A.P.; and Meyer, C.M. Selection of Input Variables for SSME Parameter Modeling Using Genetic Algorithms and Neural Networks. To be presented at *Fourth Annual Space System Health Management Technology Conference*, Cincinnati, November 17-18, 1992.

18. Roth, P. *Computer Program Contract End Item, Flight 4C Configuration, Space Shuttle Main Engine Controller Operational Program, Part 1.* CP406R0001, Revision F, Rockwell International/Rocketdyne Division, November 1988.

PID Number	PID Description	HPOT Discharge Temperature	HPFT Discharge Temperature
17	MCC Coolant Discharge Press.		x
40	FPOV		x
42	OPOV	x	
58	FPB Chamber Pressure		x
59	PBP Discharge Pressure	x	
94	PBP Discharge Temperature	x	
209	HPOP Inlet Pressure	x	
225	HPFP Inlet Temperature		x
233	HPOT Discharge Temperature		x
480	OPB Chamber Pressure	x	
1205	Engine Fuel Flowrate		x
287-63	MCC Pressure: Desired-Actual	x	x
	Average Value of Output	x	x

Table 1. Variables that appear as neural network inputs for the two modeled parameters.

Test Firing	mean error (deg R)	error standard dev. (deg R)	maximum percent error	maximum error(deg R)
B1061	-10.1	13.4	5.6	77.1
B1062	-12.4	13.9	5.0	59.0
B1066	-4.8	13.0	6.1	73.8
B1067	-16.2	15.6	5.4	69.8
B1069	15.0	16.7	6.2	72.8

Table 2. The performance of the HPOT discharge temperature model on the validation test firings.

Test Firing	mean error (deg R)	error standard dev. (deg R)	maximum percent error	maximum error (deg R)
B1061	-2.7	5.6	1.7	26.6
B1062	4.1	4.7	1.4	22.6
B1066	5.2	5.7	1.6	23.8
B1067	14.9	8.4	2.0	32.5
B1069	19.6	7.8	2.5	40.5

Table 3. The performance of the HPFT discharge temperature model on the validation test firings.

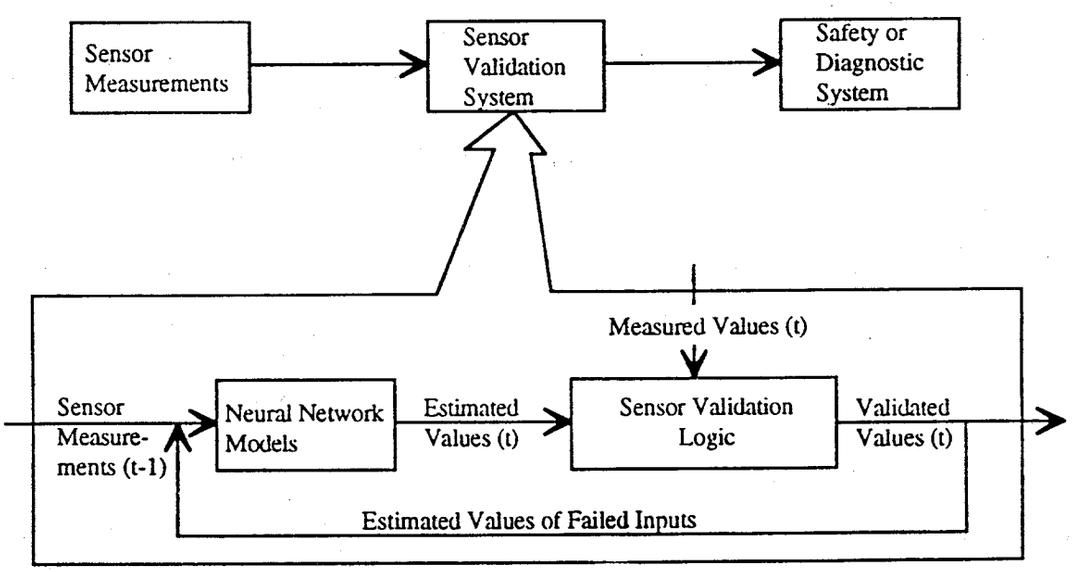

Figure 1. Major features of a sensor validation system based on neural network models; the sensor validation module passes sensor health information to a safety system or post-test diagnostic system.

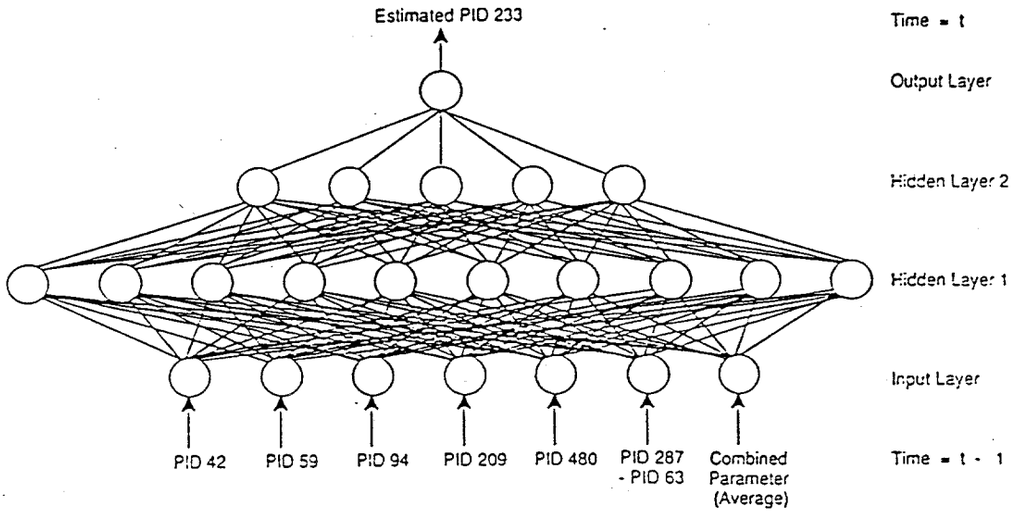

Figure 2. The neural network architecture used to model the HPOT discharge temperature. Input parameter PID numbers are shown as well as all connections between layers.

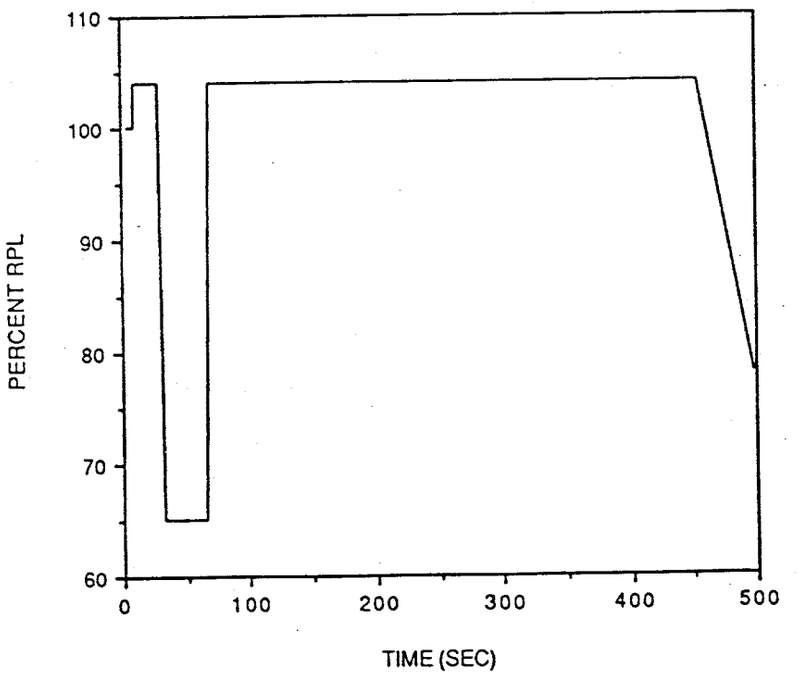

Figure 3. Power-level profile for validation test firing B1066.

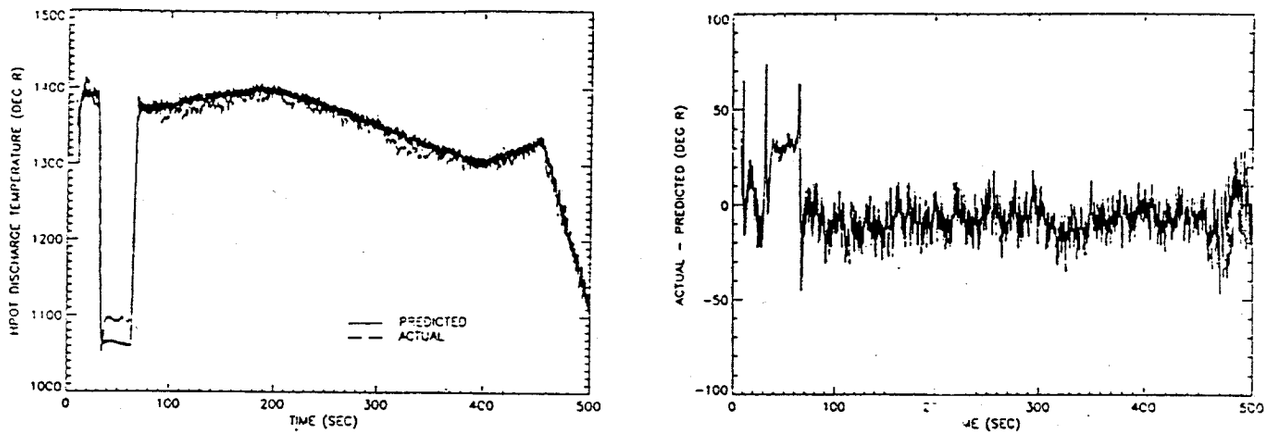

Figure 4. The performance of the HPOT discharge temperature network on validation test firing B1066: (a) actual and predicted values as a function of time and (b) the error, or difference between actual and predicted values.

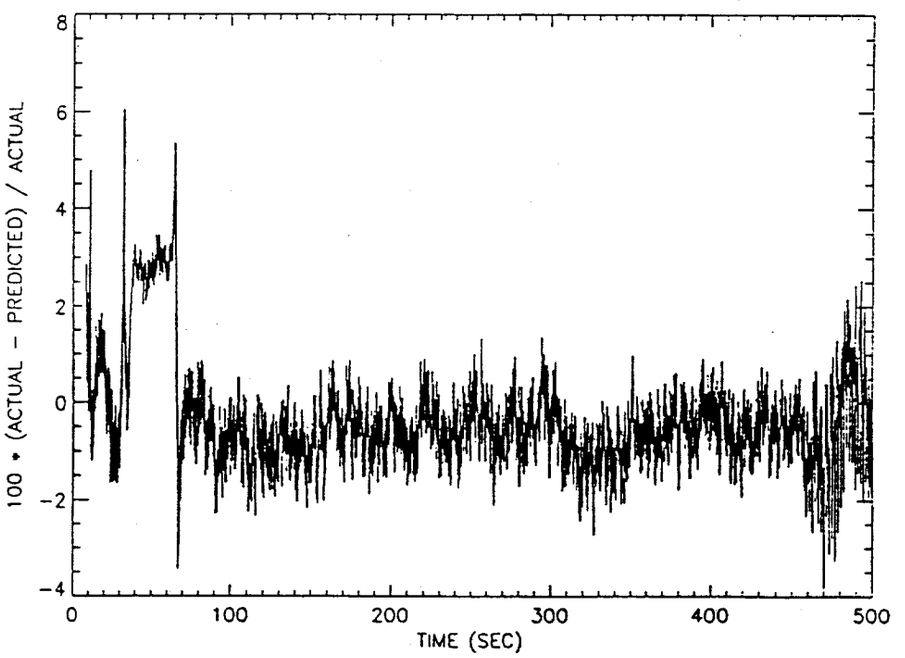

Figure 5. Percent error as a function of time for the HPOT discharge temperature network on test firing B1066.

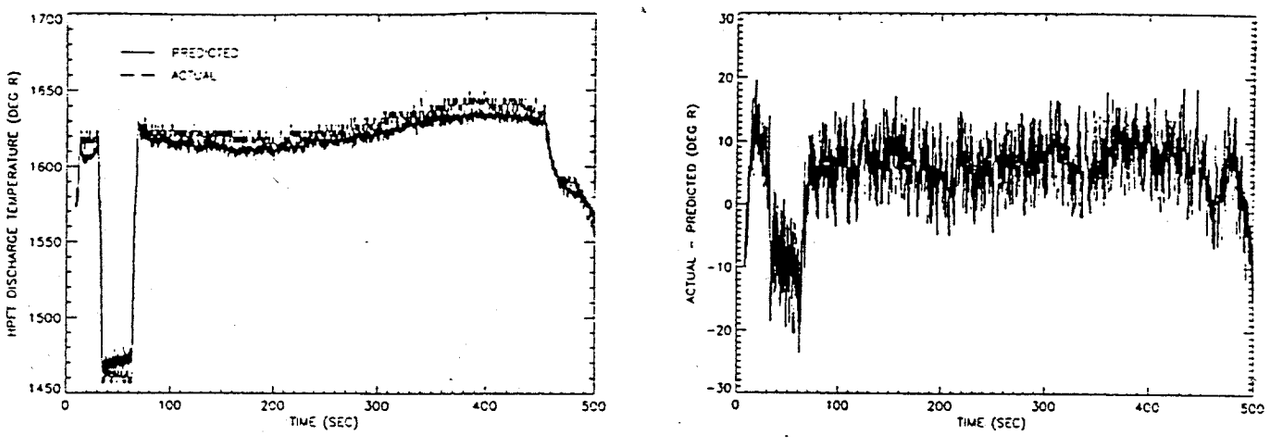

Figure 6. The performance of the HPFT discharge temperature network on validation test firing B1066: (a) actual and predicted values as a function of time and (b) the error, or difference between actual and predicted values.

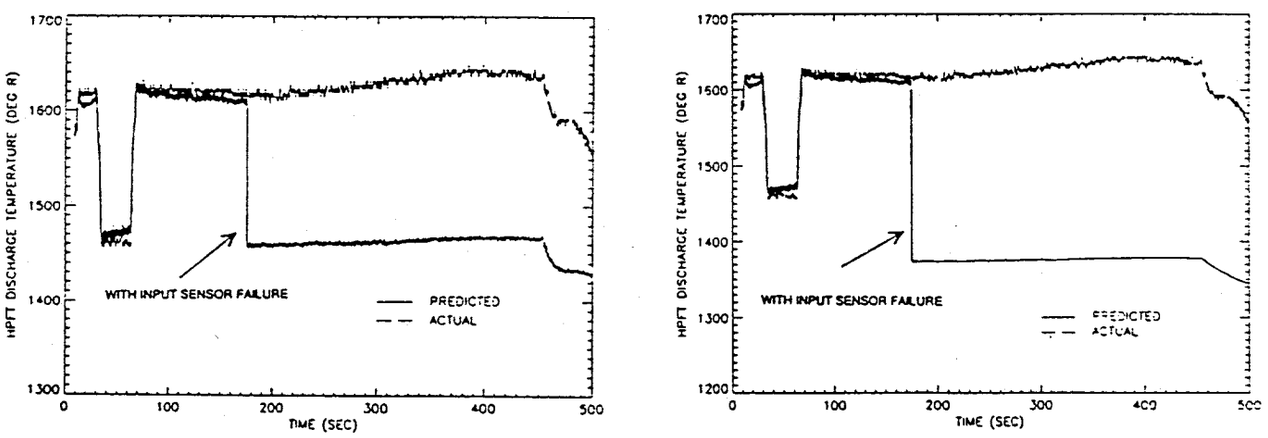

Figure 7. The performance of the HPFT discharge temperature network with an input sensor failure injected at t=175 sec: (a) failure of the HPOT discharge temperature and (b) failure of the MCC coolant discharge pressure. Nominal data was taken from validation test firing B1066.

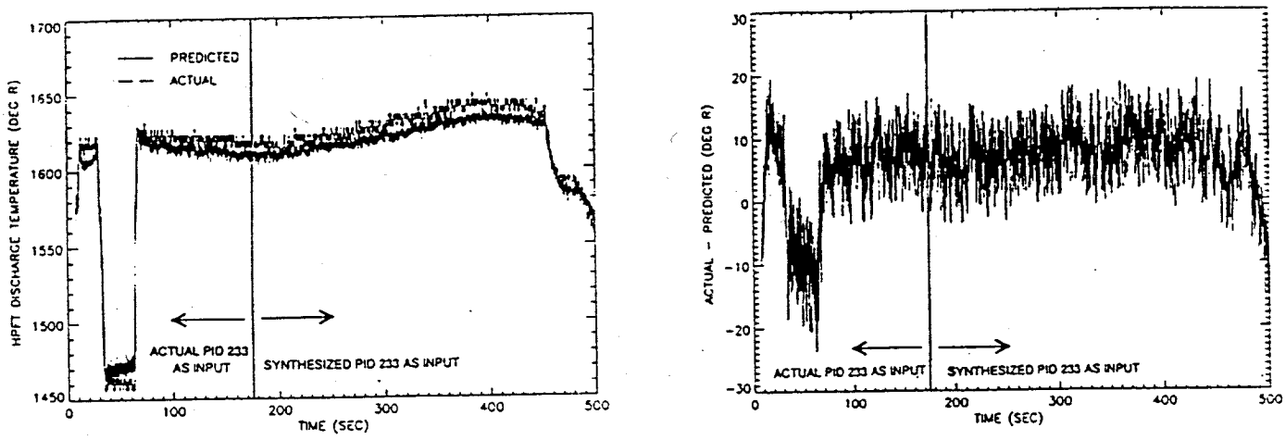

Figure 8. The performance of the HPFT discharge temperature model when synthesized data was used for the HPOT discharge temperature input beginning at t=175 sec: (a) actual and predicted values as a function of time and (b) the error, or difference between actual and predicted values.